# Impinging Shock Wave Boundary Layer Interactions Control With Shock Control Bumps

Bulut, Jane; Schrijer, Ferdinand F.; van Oudheusden, Bas W.

**DOI**
10.2514/6.2024-4526

**Publication date**
2024

**Document Version**
Final published version

**Published in**
AIAA Aviation Forum and ASCEND 2024

AIAA Aviation Forum and ASCEND co-located Conference Proceedings
29 July - 2 August 2024, Las Vegas, Nevada
AIAA AVIATION FORUM AND ASCEND 2024
10.2514/6.2024-4526

# Impinging Shock Wave Boundary Layer Interactions Control with Shock Control Bumps

Jane Bulut*, Ferry Schrijer† and Bas van Oudheusden‡
*Delft University of Technology, 2629 HS Delft, The Netherlands.*

**In this experimental study, the effect of three-dimensional shock control bumps (SCBs) on impinging-reflecting shock wave/boundary layer interactions (SWBLI) is investigated as a passive control method. The aim is to develop an understanding of the influence of such devices on the interaction structure by studying the position of the bump with respect to the shock-impingement location. The experiments were conducted in the ST-15 wind-tunnel at the Delft University of Technology for fully developed turbulent boundary layer conditions with $Re_\theta$ of 21.8 x $10^3$ and Mach number of 2. The effectiveness was assessed by examining the size of the separated flow region, as well as the downstream boundary layer velocity profile. Stereo-PIV was employed as the main diagnostic method to characterise the three-dimensional flow field. Additionally, the effect of shock impingement location on the unsteady interaction dynamics was examined by analyzing the separation size and reflected shock foot position in the instantaneous flow. The investigation revealed the significance of the shock impingement location in terms of control effectiveness. Nevertheless, placement of the bump in the interaction region substantially decreased the probability of flow separation even in off-design conditions when compared to the uncontrolled interaction.**



## I. Introduction

Shock wave boundary layer interactions (SWBLI) are a fundamental aspect of high-speed aerodynamics, as they describe the complex interplay between the compressible nature of the flowing fluid and the viscous effects near solid surfaces. These interactions have a significant impact on the performance of high-speed vehicles, potentially leading to flow separation, elevated surface heating, and unsteady pressure loads, all of which can degrade vehicle stability, control, and structural integrity.

Over the past seventy years, significant progress has been made in understanding the underlying physics of these interactions, driven by experimental and computational research efforts [1]. A remarkable part of the research is focused on the investigation of possible control methods to suppress the undesired effects of the SWBLI. While some control methods were designed to achieve control by means of changing the interaction structure, others aimed to make the boundary layer more resistant against separation. Boundary layer bleed is an example of the latter. By removing the low-momentum portion of the boundary layer through a cavity or porous surface, a fuller and more resistant boundary layer is pursued [2],[3],[4]. Another approach to energize the boundary layer involves using vortex generator devices in the sub-boundary layer level of the flow. Such devices are generally placed upstream of the interaction to increase the mixing of the boundary layer and therefore strengthen it against flow separation [5], [6], [7].

An alternative method to alleviate the unfavourable effects of the interaction is modifying the interaction structure to reduce shock strength[8], [9]. Due to their geometry, shock control bumps are well suited for this purpose when they are placed underneath the interaction. The bump geometry generates quasi-isentropic compression waves upstream of the shock impingement and results in a $\lambda$-shock configuration. The flow passing through these isentropic compression waves gradually decelerates; thus the abrupt effects that would have been caused by a stronger interaction are alleviated.

Various studies have assessed the effectiveness of such shock control bump strategies, notably for normal shock wave boundary layer interactions. In early studies, SCBs are found to be effective to reduce the wave drag under design conditions [10], while indicating restricted operational range. Moreover, it might indicate potential negative effects in off-design conditions. To address this, the use of an array of 3D SCBs has been suggested [11], [12]. Research on

*PhD Candidate, Aerodynamics Section, Department of Flow Physics and Technology, J.Bulut@tudelft.nl.
†Assistant Professor and Scientific Director of Flow Physics and Technology Laboratory, Aerodynamics Section, Department of Flow Physics and Technology.
‡Associate Professor, Aerodynamics Section, Department of Flow Physics and Technology.

3D SCB has shown its effectiveness in reducing wave drag and indicated strong evidence of streamwise vortex pair formation downstream of the bump geometry [13][14], [15].

The effectiveness of SCBs is also subject to the shock impingement location on the bump surface. In [13] Ogawa et al. investigated different 3D bump geometries and observed the dependence of the shock structure in relation to the impingement location on the bump surface. It was found that when the shock impinges on the upstream part of the bump, re-accelerated flow can create a "supersonic tongue" downstream which induces undesired secondary shock structures and an increase in the wave drag might occur [13]. In contrast, a downstream impinging shock can cause a secondary $\lambda$-shock structure formation due to the expansion of the flow passing over the crest of the bump.

Whereas most studies on the effects of SCBs have been for normal shock wave boundary layer interactions, as referred to above relatively limited research has focused on the flow structures generated by the combination ofshock control bumps and oblique SWBLIs at supersonic conditions. Considering the shape of the SCB, its effect is suggested to downsize the separation by "filling" the separation bubble with the bump structure. Also, (partially) replacing the separated flow region by the solid form of the SCB may be expected to restrict the dynamics of the separation region, thereby reducing the overall interaction unsteadiness. In addition, the streamwise vortices introduced to the downstream of the interaction by the 3D SCB, as well as the gradual flow expansion caused by the tail portion of the bump would promote to a faster flow recovery and provide a fuller velocity profile with respect to the uncontrolled case.

In this work, an experimental study is carried out to improve the understanding of the flow physics associated to the application of 3D SCBs in oblique shock wave turbulent boundary layer interactions. More in particular, the effects of the SCB and the influence of different relative shock impingement locations, on the unsteady dynamics of the SWBLI are investigated. Quantitative information on the three-dimensional flow field is obtained from stereo-PIV measurements and with this data statistical flow characteristics are analyzed. The effectiveness assessment is performed through the quantification of the separation probability and size. In addition, the effect of different impingement locations on the unsteady separation shock dynamics is investigated.



## II. Experimental Arrangement

### A. Flow facility and experimental investigation setup

The experiments are carried out in the ST-15 blow-down supersonic wind tunnel of Delft University of Technology. The test section has dimensions of 150 mm x 150 mm and has glass windows in the side walls to allow optical access. The tunnel is operated at a Mach number of 2, a total pressure $p_0$ of 3 bars and a total temperature $T_0$ of approximately 290 K. Giepman et al.[16] investigated the effects of location and size of micro-ramp vortex generators in the same facility at similar operating conditions and have also documented undisturbed boundary layer parameters. A summary of the main flow conditions is given in Table 1.

**Table 1 Experimental conditions and undisturbed boundary layer properties [7]**

| Parameter | Value | Parameter | Value |
|---|---|---|---|
| $M_\infty$ | 2.0 | $\delta_i$ | 0.63 |
| $U_\infty$ [m/s] | 520 | $\theta_i$ | 0.52 |
| $P_0$ [N/m$^2$] | 3 x $10^5$ | $H_i$ | 1.23 |
| $T_0$ [K] | 290 | $Re$ | 42 x $10^6$ |
| $\delta_{99}$ [mm] | 5.2 | $Re_\theta$ | 21.8 x $10^3$ |

The bottom wall of the wind tunnel test section, where the boundary layer thickness is approximately $\delta_{99}$=5.2mm [7], is used to assess the uncontrolled flow field. Subsequently, a shock control bump is installed on this wall with double sided adhesive tape. For all the cases, the incident shock was generated by installing a 12 degree shock generator.

In this study, two main flow diagnostic methods are used: high-speed Schlieren visualization and stereoscopic PIV (sPIV). High-speed Schlieren is used to establish the SWBLI structure and resolve its dynamics. A LaVision ProHS camera is used with an acquisition frequency of 2800 Hz, which is sufficient to resolve the major separation shock unsteadiness. However, this technique is affected by the spanwise integration of the density gradient, which brings out some limitations in decoupling the dynamics of the uncontrolled and controlled part of the test section.

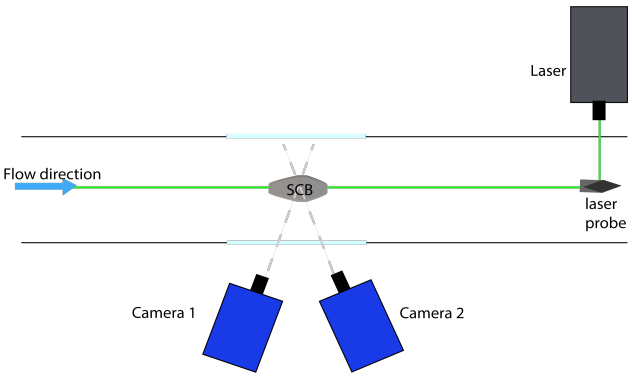


**Fig. 1 Setup of sPIV experiments.**

To capture the three-dimensional nature of the flow field resulting from the SCBs, sPIV measurements were employed. The set-up for the sPIV is shown schematically in Fig. 1, indicating two LaVision sCMOS cameras. On both cameras a 60 mm Nikkor objective was used with f# set to 8. In view of the configuration of the system, there is an offset angle between the lens plane and the image plane, and a Scheimpflug adapter was added on each lens to impose a collinear condition on the lens and sensor plane. To increase the data acquisition and processing speed, cropping was applied to the images. This resulted in a Field of View (FOV) of 141.5x41.5 mm and a digital resolution of 19 pixels/mm. For the illumination, a Quantel Evergreen double-pulsed Nd:YAG laser is used, operating at a pulse energy of 200 mJ/pulse with a repetition rate of 15 Hz. For all the measurements the pulse separation is set to 1 $\mu$s. Measurements were carried out in the symmetry plane of the bump which corresponds to the symmetry plane of the test section.

Data acquisition and processing have been performed in DaVis 8.4.0. As the first step, a Butterworth high-pass filter is applied to filter the reflections. Additionally, for the preprocessing the particle intensity was normalized using min/max filtering. Next, a multi-pass cross-correlation with 48 x 48 pixels and 24 x 24 pixels respectively, with 75% overlap was applied resulting in a vector pitch of 0.3 mm. As final step, the universal outlier detection approach was applied, as implemented in DaVis. Statistics of the velocity vector field, in terms of average and standard deviation, were also obtained through DaVis. To do so, a requirement of having at least 100 source vectors at each position to compute results is implemented.

### B. Shock control bump specifications

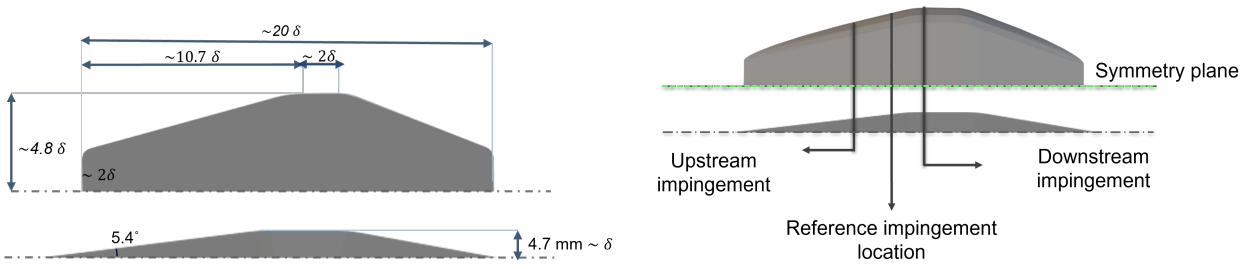


(a) *Geometrical parameters of SCB.*

(b) *Shock impingement points on bump from top and side view.*

**Fig. 2 SCB geometrical dimensions and shock impingement points on the bump surface.**

Bruce and Colliss indicated in their review [17] that most of the research on SCBs agrees that the optimum performance is achieved when the bump height is of the order of the boundary layer thickness height. While designing the geometry of the bump for the current study this guideline has been followed. Accordingly, the height at the bump crest has been selected as 4.7 mm while the ramp angle is set to 5.4 °. The bump was installed on the wind tunnel lower wall such that the symmetry plane of the bump coincides with that of the test section. Geometry effect of the SCB

on its control effectiveness has been investigated for its use in supersonic engine inlet and transonic wings [18], [13]. The wedge roundness, tail length, roughness, bump crest height and width are considered among the most relevant geometrical parameters. In light of the findings of mentioned studies [18], [13] a rounded edge bump was adopted. 3D printing is used to produce the bump geometry and by sanding the surface of it is smoothed.

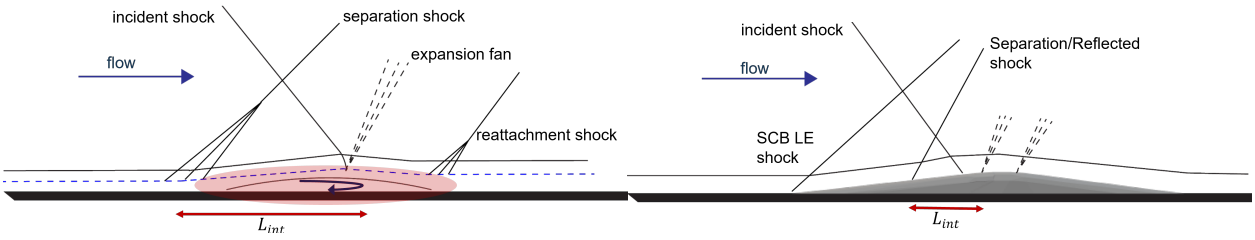


(a) *SWBLI structure.* (b) *Interaction structure with bump.*

**Fig. 3 Interaction scheme with and without the bump.**

The shock impingement location on the bump surface has been introduced as a crucial criteria to determine the efficiency of the bump. Ogawa et al. [13] defined an optimum location for shock impingement as the one that results in the largest $\lambda$-shock structure without introducing secondary shocks. When the shock is positioned further upstream of this location it is expected to introduce a secondary shock system as a result of the re-expansion of the flow after the initial shock interaction. On contrary, when the shock impinges downstream of the defined optimum location, the supersonic flow region behind the $\lambda$-shock foot accelerates due to the expansion over the bump crest which can lead to secondary shock structures as well as flow separation. In [19] Bruce and Babinsky revealed that 10 to 15% difference in the shock position around the crest has significant effects on the flow.

For this investigation, three inviscid impingement locations on the bump were defined (See Fig. 2b). A first control impingement location is defined 1.5 $\delta$ upstream of the first point where the bump has a maximum height. This corresponds to a 9.2 $\delta$ distance from the leading edge of the bump. Additionally, impingement locations as being 1.5 $\delta$ downstream and 1 $\delta$ upstream of this point are investigated. These will be referred to as downstream impingement location and upstream impingement location in the following of the discussion. The incident shock impingement locations were decided regarding the previously mentioned studies which have been conducted on normal shock-boundary layer interactions [14], [20]. In this way, the sensitivity of the location of the shock control bumps can be investigated for flow control.

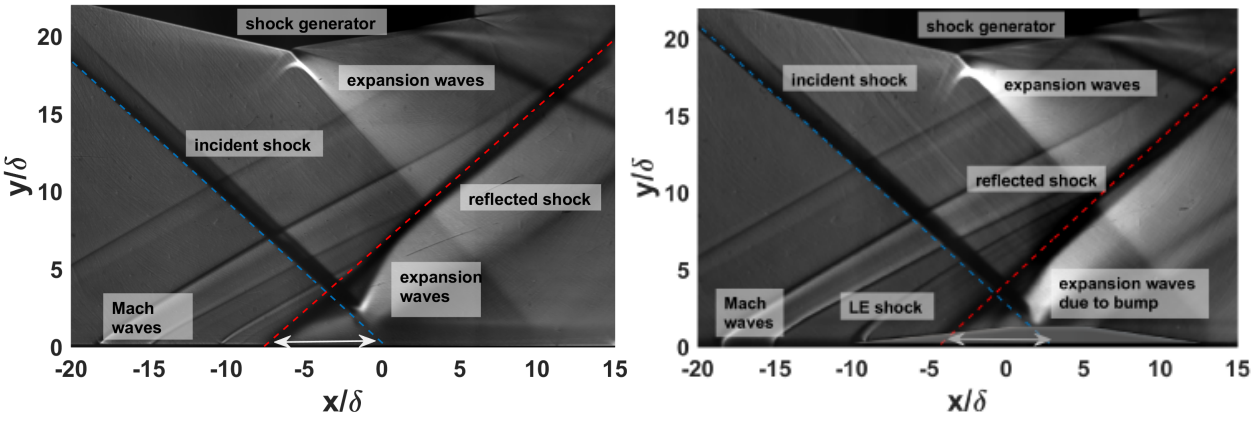


(a) *Uncontrolled interaction.* (b) *Controlled interaction.*

**Fig. 4 Average flow field obtained from Schlieren measurements.**

# III. Results

## A. Interaction structure with and without control

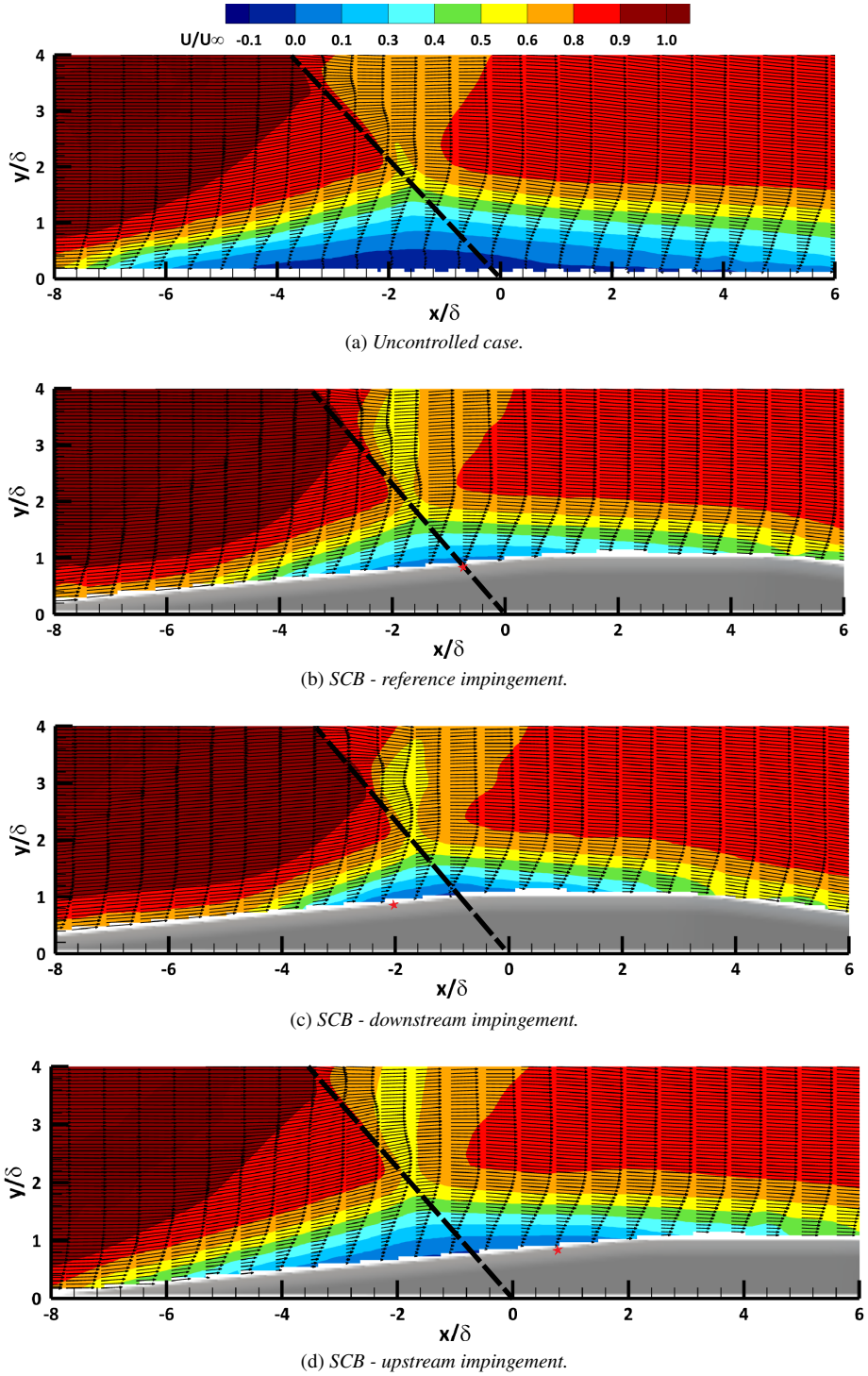


(a) *Uncontrolled case.*

(b) *SCB - reference impingement.*

(c) *SCB - downstream impingement.*

(d) *SCB - upstream impingement.*

**Fig. 5 Streamwise velocity contour of mean flow field (impinging shock wave is represented by the dashed line and red star indicates the reference impinging point on the bump surface).**

In Fig. 4 images obtained from Schlieren visualization show the global features of the uncontrolled and controlled

interactions, respectively. The incident shock is generated by a 12° shock generator and the extrapolated, theoretical intersection location with the wall is defined as the origin for the x-coordinate. The reflected shock is formed approximately $7\delta$ upstream of the impinging location of the incident shock for the case of the uncontrolled interaction. Downstream of the interaction, it can be seen that the boundary layer has increased in thickness. The different shock impingement locations, as described in Section II.B, were achieved by translating the shock generator along the longitudinal direction.

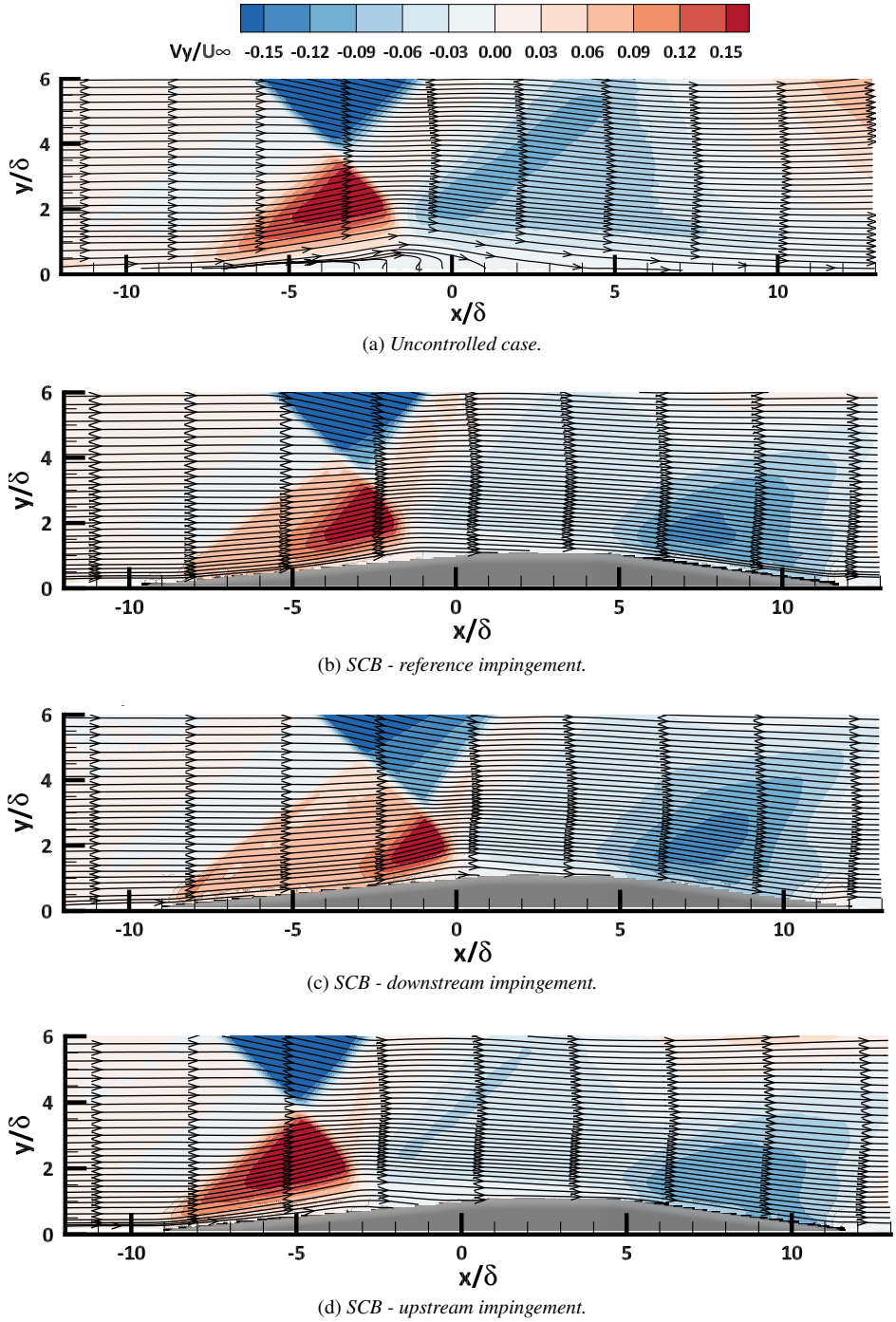


(a) *Uncontrolled case.*

(b) *SCB - reference impingement.*

(c) *SCB - downstream impingement.*

(d) *SCB - upstream impingement.*

**Fig. 6 Wall normal velocity contour of mean flow field.**

Mean flow organizations obtained from PIV measurements are represented in Fig. 5 and Fig. 6. In the plots the

coordinate system is defined with x being in the streamwise direction and y being normal to the wall. The spatial coordinates are normalized to the thickness of the incoming undisturbed boundary layer, $\delta$. The origin of the coordinate system is defined as the inviscid impingement location of the incident shock on the wall.

The mean streamwise velocity of the uncontrolled and controlled cases is shown in Fig. 5. Velocity vectors are plotted over the mean streamwise velocity color contours of the overall field of view. The location of the inviscid impingement on the wall is chosen consistently as the origin for all cases. Velocity vector profiles reveal differences particularly in the interaction region. The strong adverse pressure gradient imposed by the shock impingement causes thickening of the boundary layer and results in flow separation for the uncontrolled interaction. (see Fig.5). Meanwhile, the boundary layer becomes thicker as a result of the interaction, while the mean flow field remains attached (i.e., no reverse flow) for the cases with bump.

Although the boundary layer could not be fully resolved due to reflections in the region close to the wall, the controlled interaction indicates a fuller velocity profile in the region that corresponds to the interaction of the uncontrolled case. In particular, the reference and downstream impingement cases show a fuller velocity profile for a longer distance when approaching the incident shock impingement location. In addition, the flow expansion introduced by the bump geometry positively contributes to the flow recovery downstream of the interaction. Consequently, lower momentum flow resulted by the interaction is confined in a smaller region in the controlled interactions.

The vertical velocity contour of the averaged flow field is complemented with the streamlines obtained from two-dimensional velocity gradients (see Fig.6). Streamlines don't indicate any reversed flow for the controlled cases, while the streamline layout for the controlled case clearly indicate a flow reversal. In addition, the formation of a weak shock originating from the leading edge of the bump is clearly seen, especially in the cases of the control impingement and the downstream impingement location. The ramp face of the bump deflects the upstream supersonic flow, and hence it is expected to induce shock wave formation. Therefore, in the cases where the shock is sufficiently downstream of the leading edge, the effect of this weak shock can be seen in the flow. At the location where the leading edge shock meets the incident shock, an additional shock-shock interaction occurs in the flow. For the upstream impingement case, on the other hand, the reflected and LE shocks appear to be merged, yielding a time-average shock structure that is quite similar to that of the uncontrolled interaction.

Individual contributions of the streamwise and the wall-normal velocity fluctuations to the local turbulence level are depicted in Fig. 7. Although the streamwise velocity fluctuation is highest in the separated region and shear layer, strongest fluctuations in the wall normal component are reached around the reflected shock, indicative of its degree of unsteadiness. In the boundary layer downstream of the interaction, large-scale vortex shedding also promotes a high level of fluctuations in the wall normal velocity. Highest streamwise velocity fluctuations reached in the interaction is limited to a smaller region of the flow when the bump is introduced to the flow. It can be seen that when the incident shock impinges upstream on the bump surface, fluctuations in streamwise velocity can still be seen in a relatively large region. However, the level of highest fluctuation is lower in comparison to the uncontrolled interaction. In all cases, fluctuations of the wall-normal velocity around the reflected shock are measure of its unsteady nature. As a consequence of that, in reference and downstream impingement cases significantly lower level of fluctuations are observed indicating a more steady behaviour of the reflected shock.

In Fig. 8, turbulent intensity in the interaction region is plotted for the uncontrolled and controlled interactions. Turbulent intensity is an indication of the overall fluctuation levels of the velocity components over the mean flow. In the uncontrolled interaction, reflected shock exhibits more pronounced fluctuations as a consequence of variation of the its position. On the other hand, incident shock is well known to have stationary characteristics and fluctuations that are observed in the vicinity of the incident shock are due to measurement uncertainties. Additionally, high levels of fluctuations observed in the regions close to the wind tunnel wall and bump surface are consequences of the high reflections occurring close to these surfaces.

### B. Effect on the interaction dynamics and flow separation

Analyzing the mean flow is not conclusive to deduce information on the separation state of the flow. Due to its breathing behaviour, separation bubble repetitively dilates and collapses. Therefore, a better understanding on the separation dynamics requires the analysis of instantaneous flow field information. There is a subtle distinction between the separation bubble and flow reversal, regardless of their commonly interchangeable use. Flow reversal is identified through the determination of zero-velocity iso-line, whereas the presence of a separation bubble necessitates the recognition of a dividing streamline [21]. Therefore, introducing the concept of statistical occurrence, specifically the "separation (or: reverse-flow) probability," offers a pragmatic and less sensitive approach to assess the severity of sep-

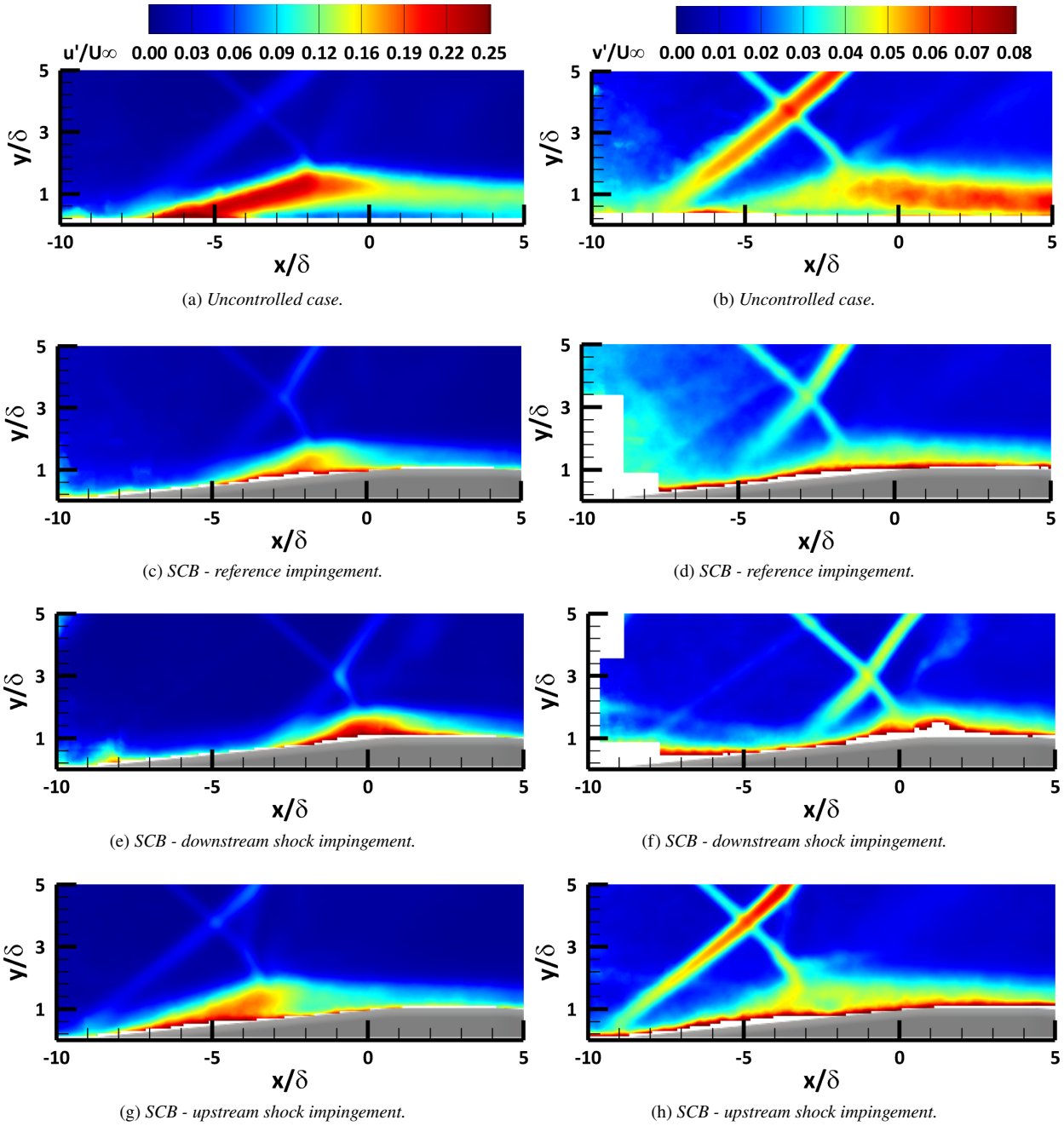


(a) *Uncontrolled case.*

(b) *Uncontrolled case.*

(c) *SCB - reference impingement.*

(d) *SCB - reference impingement.*

(e) *SCB - downstream shock impingement.*

(f) *SCB - downstream shock impingement.*

(g) *SCB - upstream shock impingement.*

(h) *SCB - upstream shock impingement.*

**Fig. 7 Turbulent intensity in the interaction region where.**

aration in a fluid flow. This methodology not only enhances the characterization of separation phenomena but also facilitates a comparative analysis across diverse cases.

In this study, 900 instantaneous images are obtained for each case. From these images the local separation probability is calculated for each point on the selected window on each image. As explained previously, the separation criteria is connected to the occurrence of reversed flow. Fig.9 compares the spatial distribution of the separation probability, $P_{sep}$, for the different interaction configurations. The percentages represents the time fraction that reversed flow is encountered at that specific location.

Without applying any control method, more than 70% of the time flow is reversed in the region adjacent to the wall.

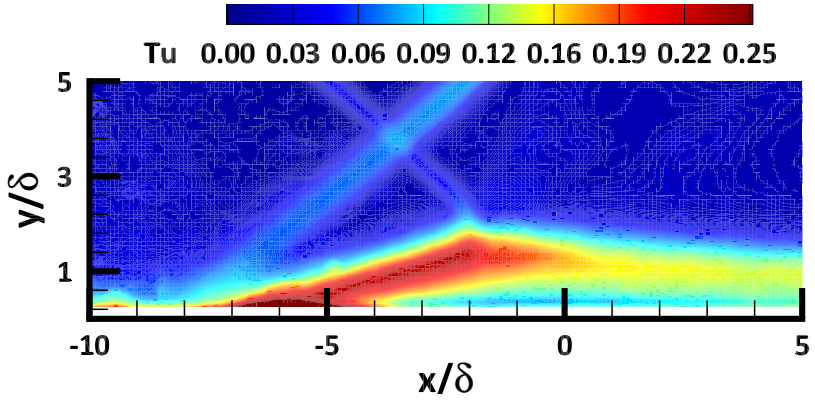


(a) *Uncontrolled case.*

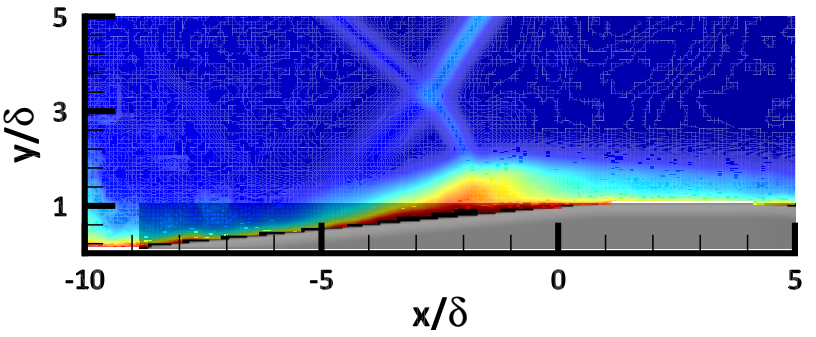


(b) *SCB - reference impingement.*

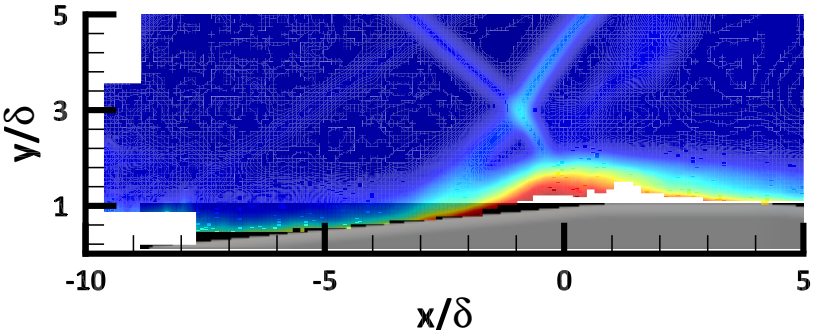


(c) *SCB - downstream shock impingement.*

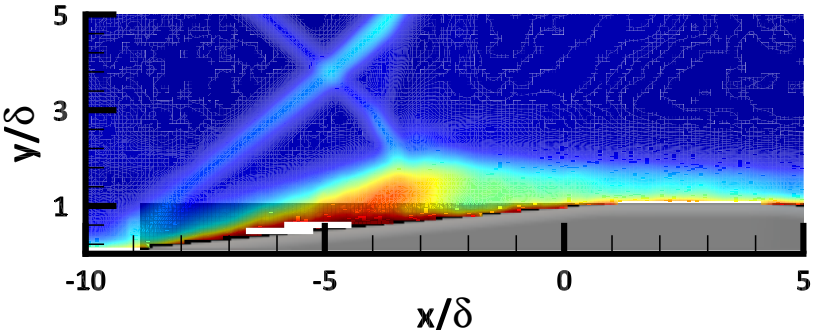


(d) *SCB - upstream shock impingement.*

**Fig. 8 Turbulent intensity in the interaction region where** $Tu = \sqrt{u'^2 + v'^2}/U_\infty$.

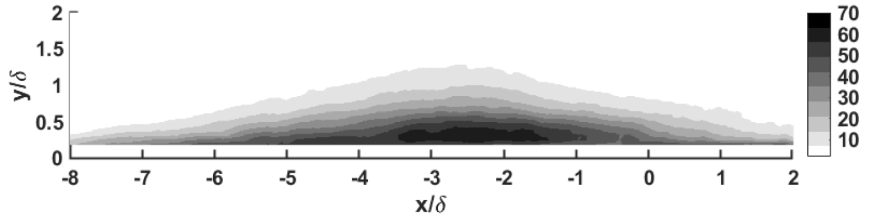


(a) *Uncontrolled case.*

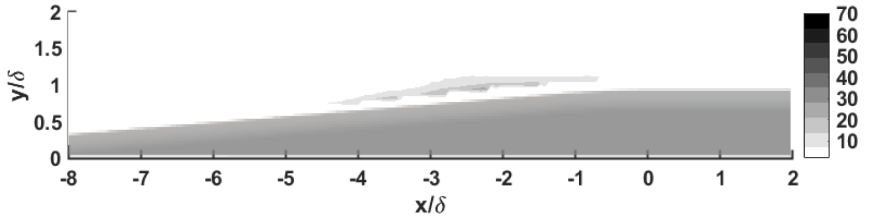


(b) *SCB - reference impingement.*

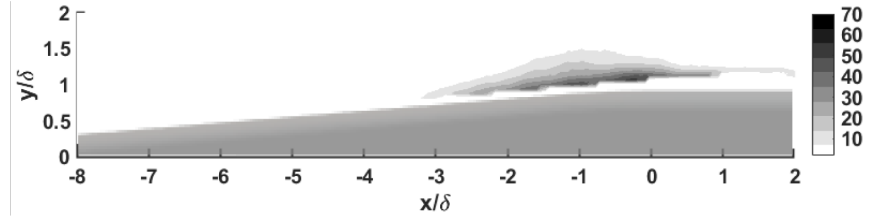


(c) *SCB - downstream impingement.*

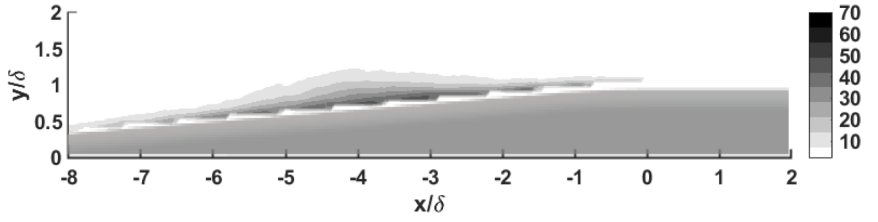


(d) *SCB - upstream impingement.*

**Fig. 9 Separation probability map.**

All the cases with bump exhibit a decrease in the peak value of the $P_{sep}$. The flow reversal occurrence in the reference case, where the shock impingement location is set to $1\delta$ upstream of the bump crest, it is limited to a maximum of 10% in a very limited region of the flow. When the shock impingement is moved to the upstream position, the maximum $P_{sep}$ is increased to approximately 40% and the region that the separation can be observed is larger in comparison with the other controlled interaction cases. Nevertheless, separation in all the cases with bump is confined in much smaller area than it is observed for the uncontrolled interaction case.

As extensively reported in literature, the reflected shock oscillation is associated with a breathing motion of the separation bubble [22]. Introducing the bump is aimed to remove the separation from the flow. When the separation is annihilated or the bubble is significantly reduced in size, it is expected to see accordingly a reduced oscillatory motion in the reflected shock. To investigate this, a shock detection algorithm was applied to the PIV results. The shock detection is performed in the region outside the boundary layer. Velocity fluctuations around the reflected shock in the outer flow region and those of the shock foot inside the boundary layer have been reported to be correlated. Souverein et al. [23]; showed that even though the behaviour of the reflected shock foot is affected by the passages of turbulent structures in the incoming boundary layer, low frequency unsteadiness observed at this region is highly correlated with the oscillating motion of the reflected shock in the outer flow.

With the shock detection algorithm, the relative displacement of the shock wave regarding to the shock location in

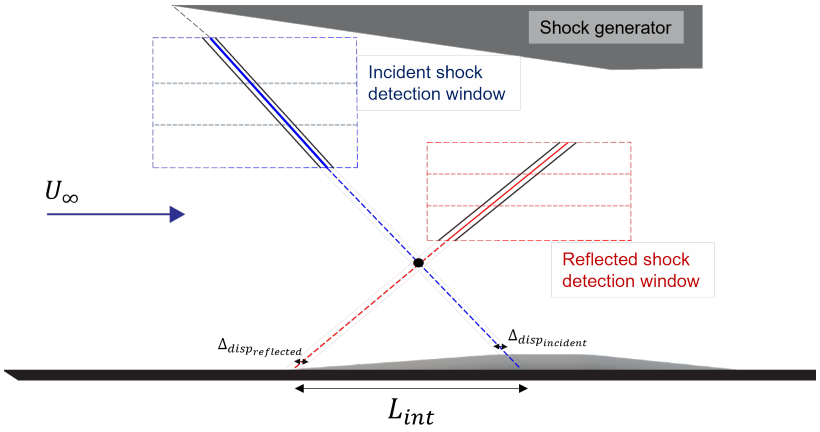


**Fig. 10 Shock detection window selection.**

the reference frame is obtained. Therefore as initial step, a reference image is selected and both incident and reflected shock positions are determined. The maximum velocity gradient is chosen as the criteria to locate the shock positions. The corresponding detection windows for both shock waves are shown in Fig.10. In addition to the main detection criteria, a filtering is applied to avoid the selection of spurious points for the shock location, by limiting the search region with respect to the mean shock location. Once the shock points detected, the instantaneous shock line is obtained by applying a linear fit. Inviscid impingement point of the incident shock and the originating point of the reflected shock is computed by extrapolating the obtained shock lines towards the wall.

After the reference shock position is obtained, the relative position of the shock is derived by applying a cross correlation between the reference image and the target instantaneous image. This process is also done in the selected shock detection windows (see Fig.10). In order to better represent the shock motion, the detection window is divided into 3 segments in y-direction and each of them are cross correlated with the corresponding one in the reference image. Once the trend of the shock position offset is obtained, the corresponding shock foot displacement on the wall is computed for each instantaneous image. In addition, to reach a higher accuracy in the detection process, sub-pixel cross correlation is also employed.

**Table 2 Standard deviation of the shock positions on the wall and interaction properties**

| Cases | $\text{std}_{refl}$ $[\delta]$ | $\text{std}_{L_{inc}}$ $[\delta]$ | $L_{int}$ $[\delta]$ |
|---|---|---|---|
| Uncontrolled | 0.54 | 0.55 | 8.8 |
| Reference impingement | 0.20 | 0.17 | 7.4 |
| Upstream impingement | 0.43 | 0.45 | 8.8 |
| Downstream impingement | 0.30 | 0.30 | 6.5 |

The incident shock is found to be highly steady for all of the cases, with the unsteadiness of the impingement location is obtained as being approximately $0.04\delta$ for all cases. This agrees with the observations in other studies [24], [25], [26]. As the incident shock wave was tracked in the outer flow, it is expected to have a steady nature, independently of the interaction dynamics. On the other hand, the elevated standard deviation values of the reflected shock location suggests a strong unsteady behaviour for the uncontrolled interaction. The reflected shock is found to be more steady in all the controlled cases in comparison with the uncontrolled case. In the reference impingement case, a significant reduction in the standard deviation of the reflected shock position on the wall can be seen (see Table2). Lower fluctuations in the reflected shock position indicates reduced large-scale low-frequency unsteadiness. Moreover, when the separation is annihilated or the bubble is significantly smaller in size, it is expected to see also an alleviated oscillatory motion in the reflected shock. Therefore, introducing the bump reduced the flow separation especially for the reference and downstream shock impingement cases considered.

The low frequency unsteadiness is often characterized by a dimensionless frequency, or Strouhal number [27], [28]. The Strouhal number, $St_L = fL/U_\infty$, associates the shock motion with a characteristic length of the separation. The

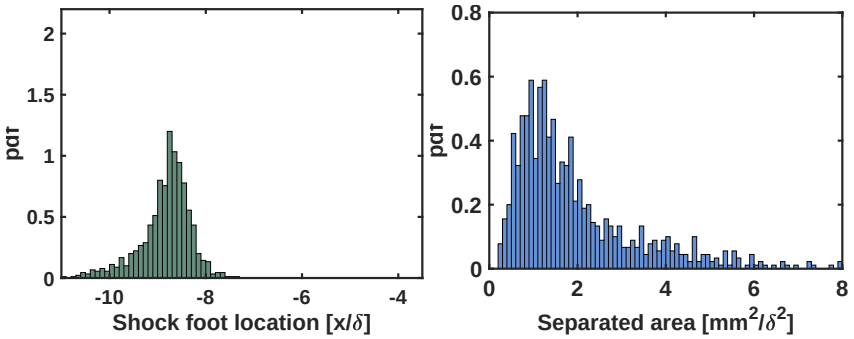


(a) *Uncontrolled case.*

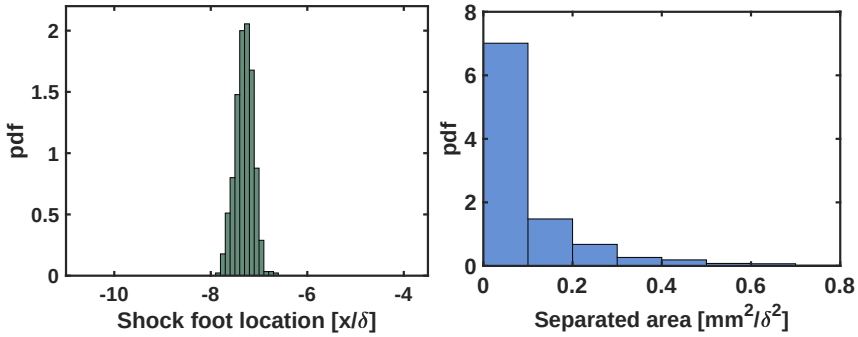


(b) *SCB - reference impingement.*

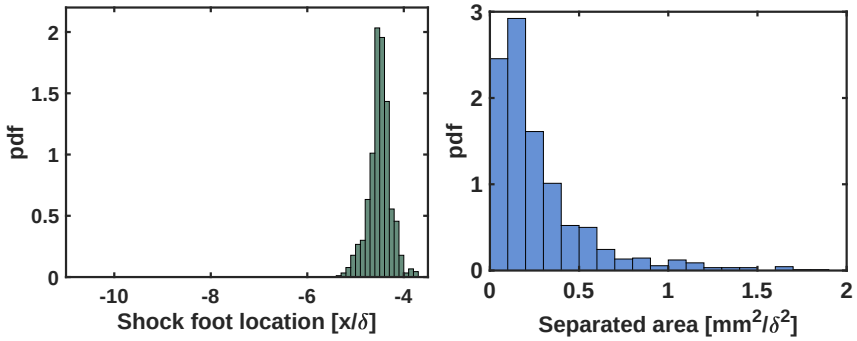


(c) *SCB - downstream shock impingement.*

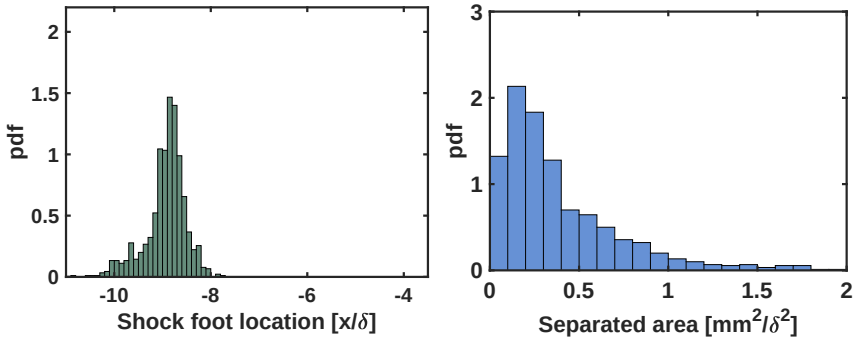


(d) *SCB - upstream shock impingement.*

**Fig. 11 Normalized pdfs of the non-dimensional reflected shock foot position in the left column (inviscid incident shock impingement is at the origin for all cases) and separation size in the right column.**

characteristic length, is commonly taken as the interaction length, which is defined as the distance from the impingement point of inviscid incident shock on the wall to the point that the reflected shock originates on the wall. The corresponding average interaction length observed in the reference and downstream impingement cases is significantly lower than the one of the uncontrolled case (see Table2). A reduction in the interaction length, hence, can be interpreted as alleviated separation. In fact, the calculated separation probability for the investigated controlled cases is significantly lower than the one of the uncontrolled case (see Fig.9). The breathing motion of the separation bubble forces the reflected shock to oscillate. With the impinging shock position remaining predominantly stationary, this also results in an alteration in the interaction length of the instantaneous flow. Where the shock excursion amplitude is higher, one could assume the separation bubble grows in size. Tracking the reflected shock revealed a shock excursion length of approximately 4 $\delta$ for the uncontrolled interaction (see Fig.11). Meanwhile the oscillation range of the reflected shock is limited to 1.5 $\delta$ in the reference impingement case. Higher values of the excursion length indicates an increased unsteadiness of the interaction region. In addition, it could also be interpreted as occurrence of larger separation size.

Spatial probability of local reversed flow occurrence is demonstrated in Fig.9. In order to acquire more information on the separation bubble behaviour, instantaneous separation size is tracked for all the cases. Having the prior knowledge of the vector pitch and number of reversed flow vectors, approximate separation size is obtained. In the second column of the Fig.11, normalized probability density distribution of the non-dimensional separation size is plotted all the investigated interaction cases. Enforcing the shock impingement at the reference point has limited the reversed flow to less than 1 unit area. Moreover, at most of the instances, the separation size is remained less than 0.2 unit area. On the contrary, separation area is observed not to be less than 0.2 unit area at any instance of the uncontrolled interaction. In addition, separation size distribution shows that reversed flow area can grow 10 times when no control is applied in comparison with the reference control case. Even though upstream and downstream impingement cases exhibit larger separation area than the reference case in some instances, all of the controlled cases seem to limit the breathing range of the separation bubble.



## IV. Conclusion

An experimental investigation has been carried out to asses the influence of the shock impingement location for the effectiveness of shock control bumps. Three shock positions are considered. The shock impingement set to approximately 1$\delta$ upstream of the crest of the bump is considered as the reference case. Two additional cases, where shock impinges more upstream and downstream of this position, are evaluated as off-design conditions.

Stereo-PIV measurements were performed to visualize the 3D flow organization. The mean flow fields obtained from these measurements showed no discernable time-average flow separation for the controlled cases. In addition, lower velocity fluctuation levels are observed in comparison with the uncontrolled interaction. This reduced the turbulence intensity in the interaction region can be attributed to removal of the flow separation. The controlled interaction cases also demonstrate a fuller boundary layer profile downstream of the interaction which can be interpreted as a healthier boundary layer flow.

The probability of separation, $P_{sep}$, was determined for all cases, including the uncontrolled case. The minimum separation probability occurs for the control impingement location case with the bump with 10% $P_{sep}$. This indicates approximately 85% improvement compared to the uncontrolled case where the maximum value of $P_{sep}$ is found 70%.

The main principle of the control with SCBs is a beneficial modification of the shock structure. It is further shown with this work that, similar as in normal SWBLIs, the shock impingement location has a significant effect on this. When the incident shock impinges significantly downstream of the bump leading edge and just upstream of the expansion introduced by the bump crest, control effectiveness reached its maximum. It is seen that when the interaction occurs in the vicinity of the bump leading edge, effectiveness of the bump is negatively affected. Nevertheless, even in the considered off-design conditions, the introduction of the bump in the interaction proved to alleviate the reflected shock unsteadiness and reduce the separation size in comparison to the uncontrolled interaction.

## Acknowledgments

This work has been carried out as part of the TEAMAero project which has received funding from the European Union's Horizon2020 research and innovation program under the grant agreement No. EC grant 860909.

# References


[1] Dolling, D. S., "Fifty Years of Shock-Wave/Boundary-Layer Interaction Research: What Next?" *https://doi.org/10.2514/2.1476*, Vol. 39, No. 8, 2012, pp. 1517–1531. https://doi.org/10.2514/2.1476, URL https://arc.aiaa.org/doi/10.2514/2.1476.

[2] McCormick, D. C., "Shock/boundary-layer interaction control with vortex generators and passive cavity," *AIAA Journal*, Vol. 31, No. 1, 1993. https://doi.org/10.2514/3.11323.

[3] Doerffer, P. P., and Bohning, R., "Shock wave – boundary layer interaction control by wall ventilation," *Aerospace Science and Technology*, Vol. 7, No. 3, 2003, pp. 171–179. https://doi.org/10.1016/S1270-9638(02)00009-3.

[4] Giehler, J., Leudiere, T., Morgadinho, R. S., Grenson, P., and Bur, R., "Experimental and numerical investigation of porous bleed control for supersonic/subsonic flows, and shock-wave/boundary-layer interactions," *Aerospace Science and Technology*, Vol. 147, 2024, p. 109062. https://doi.org/10.1016/J.AST.2024.109062.

[5] Babinsky, H., Li, Y., and Ford, C. W., "Microramp control of supersonic oblique shock-wave/boundary-layer interactions," *AIAA Journal*, Vol. 47, No. 3, 2009. https://doi.org/10.2514/1.38022.

[6] Panaras, A. G., and Lu, F. K., "Micro-vortex generators for shock wave/boundary layer interactions," , 2015. https://doi.org/10.1016/j.paerosci.2014.12.006.

[7] Giepman, R. H., Schrijer, F. F., and Van Oudheusden, B. W., "Flow control of an oblique shock wave reflection with micro-ramp vortex generators: Effects of location and size," *Physics of Fluids*, Vol. 26, No. 6, 2014. https://doi.org/10.1063/1.4881941.

[8] Bur, R., Corbel, B., and Délery, J., "Study of Passive Control in a Transonic Shock Wave/Boundary-Layer Interaction," *https://doi.org/10.2514/2.376*, Vol. 36, No. 3, 1998, pp. 394–400. https://doi.org/10.2514/2.376, URL https://arc.aiaa.org/doi/10.2514/2.376.

[9] Ashill, P. R., Fulkner, L., and Shires, A., "A novel technique for controlling shock strength of laminar flow aerofoil sections," *DGLR Bericht Proceedings*, Vol. 6(92-01-022), 1992, pp. 175–183.

[10] Sommerer, A., Lutz, T., and Wagner, S., "Design of adaptive transonic airfoils by means of numerical optimisation," *European Congress on Computational Methods in Applied Sciences and Engineering, ECCOMAS 2000*, 2000.

[11] Qin, N., Wong, W. S., and Le Moigne, A., "Three-dimensional contour bumps for transonic wing drag reduction," *Proceedings of the Institution of Mechanical Engineers, Part G: Journal of Aerospace Engineering*, Vol. 222, No. 5, 2008. https://doi.org/10.1243/09544100JAERO333.

[12] Holden, H. A., and Babinsky, H., "Shock / boundary layer interaction control using 3D devices," *41st Aerospace Sciences Meeting and Exhibit*, 2003. https://doi.org/10.2514/6.2003-447.

[13] Ogawa, H., Babinsky, H., M. Pätzold, and T. Lutz, "Shock-wave/boundary-layer interaction control using three-dimensional bumps for transonic wings," *AIAA Journal*, Vol. 46, No. 6, 2008. https://doi.org/10.2514/1.32049.

[14] Bruce, P. J., and Babinsky, H., "Experimental study into the flow physics of three-dimensional shock control bumps," *Journal of Aircraft*, Vol. 49, 2012. https://doi.org/10.2514/1.C031341.

[15] Colliss, S. P., Babinsky, H., Nübler, K., and Lutz, T., "Joint experimental and numerical approach to three-dimensional shock control bump research," *AIAA Journal*, Vol. 52, No. 2, 2014. https://doi.org/10.2514/1.J052582.

[16] Giepman, R., "Flow control for oblique shock wave reflections," Ph.D. thesis, 2016.

[17] Bruce, P. J., and Colliss, S. P., "Review of research into shock control bumps," , 2015. https://doi.org/10.1007/s00193-014-0533-4.

[18] Ogawa, H., and Babinsky, H., "Shock / boundary-layer interaction control using three-dimensional bumps in supersonic engine inlets," *46th AIAA Aerospace Sciences Meeting and Exhibit*, 2008. https://doi.org/10.2514/6.2008-599.

[19] Bruce, P. J., Colliss, S. P., and Babinsky, H., "Three-dimensional shock control bumps: Effects of geometry," *52nd AIAA Aerospace Sciences Meeting - AIAA Science and Technology Forum and Exposition, SciTech 2014*, American Institute of Aeronautics and Astronautics Inc., 2014.

[20] Bruce, P. J., Colliss, S. P., and Babinsky, H., "Three-dimensional shock control bumps: Effects of geometry," *52nd Aerospace Sciences Meeting*, 2014. https://doi.org/10.2514/6.2014-0943.

[21] Giepman, R., "Flow control for oblique shock wave reflections," Ph.D. thesis, 2016.

[22] Clemens, N. T., and Narayanaswamy, V., "Low-frequency unsteadiness of shock wave/turbulent boundary layer interactions," *Annual Review of Fluid Mechanics*, Vol. 46, 2014. https://doi.org/10.1146/annurev-fluid-010313-141346.

[23] Souverein, L. J., Bakker, P. G., and Dupont, P., "A scaling analysis for turbulent shock-wave/boundary-layer interactions," *Journal of Fluid Mechanics*, Vol. 714, 2013. https://doi.org/10.1017/jfm.2012.495.

[24] Humble, R. A., Elsinga, G. E., Scarano, F., and van Oudheusden, B. W., "Three-dimensional instantaneous structure of a shock wave/turbulent boundary layer interaction," *J. Fluids Mech.*, Vol. 622, 2009, pp. 33–62. https://doi.org/10.1017/s0022112008005090.

[25] Souverein, L. J., Van Oudheusden, B. W., Scarano, F., and Dupont, P., "Application of a dual-plane particle image velocimetry (dual-PIV) technique for the unsteadiness characterization of a shock wave turbulent boundary layer interaction," *Measurement Science and Technology*, Vol. 20, No. 7, 2009, p. 074003. https://doi.org/10.1088/0957-0233/20/7/074003, URL https://iopscience.iop.org/article/10.1088/0957-0233/20/7/074003https://iopscience.iop.org/article/10.1088/0957-0233/20/7/074003/meta.

[26] van Oudheusden, B. W., Jöbsis, A. J., Scarano, F., and Souverein, L. J., "Investigation of the unsteadiness of a shock-reflection interaction with time-resolved particle image velocimetry," *Shock Waves*, Vol. 21, No. 5, 2011, pp. 397–409. https://doi.org/10.1007/S00193-011-0304-4/METRICS, URL https://link.springer.com/article/10.1007/s00193-011-0304-4.

[27] Erengil, M. E., and Dolling, D. S., "Correlation of separation shock motion with pressure fluctuations inthe incoming boundary layer," *AIAA Journal*, Vol. 29, No. 11, 1991. https://doi.org/10.2514/3.10812.

[28] Debiève, J. F., and Dupont, P., "Dependence between the shock and the separation bubble in a shock wave boundary layer interaction," *Shock Waves*, Vol. 19, No. 6, 2009. https://doi.org/10.1007/s00193-009-0232-8.